Photo-Induced Electron Transfer Between a Reactant Molecule and Semiconductor Photocatalyst: In Situ Doping

AUTHOR(S):

Shishido, Tetsuya; Teramura, Kentaro; Tanaka, Tsunehiro

Title:

Photo-induced electron transfer between a reactant molecule and semiconductor photocatalyst - in situ doping

Author names and affiliation:

Tetsuya SHISHIDO, Kentaro TERAMURA, Tsunehiro TANAKA

Department of Molecular Engineering, Graduate School of Engineering, Kyoto University
Katsura, Kyoto 615-8510, Japan

Running title

Electron transfer between a reactant molecule and semiconductor photocatalyst

Corresponding Author

Tsunehiro TANAKA

Tel. 81-75-383-2558 Fax. 81-75-383-2561

E-mail tanakat@moleng.kyoto-u.ac.jp

Address:

Department of Molecular Engineering, Graduate School of Engineering, Kyoto University
Katsura, Kyoto 615-8510, Japan

Abstract

The possibility of the direct electron transition between the donor/acceptor level generated by adsorbed molecules and the conduction/valence band for photo-illuminated semiconductor-type metal oxide is discussed. The effective wavelength is shifted to a longer wavelength by the formation of donor/acceptor level derived from adsorbed molecule (called here "*in situ doping"*). This photo-activation mechanism by "*in situ doping*" gives us attractive ways for the removing the limit of band-gap energy, and the utilization of visible light.

Key words: in situ doping; photocatalysis; metal oxide; NH_3; alcohol; amine; CO_2.

Introduction

Photocatalysis of semiconductor-type metal oxides is generally explained in terms of band theory (the classical electron transfer mechanism) accompanied by the interaction of reactants with the photo-generated electrons and holes, and is potentially available to make the catalytic reaction proceeding at low temperature. Photocatalytic reactions on a powder of semiconductor type metal oxide involves several steps as shown in Scheme 1. Electron transfer between solid and adsorbates is one of the key steps in photocatalysis. The energy transfer excluding the electron transfer clearly discriminates between photocatalysis and photosensitizing reactions. Although it may not be generally accepted, Fox and Chan [1] has proposed that the singlet oxygen species as an active oxygen species over TiO_2 photocatalyst is formed by a couple of consecutive electron transfer reactions;

$$e^- + O_2 \rightarrow O_2^- \qquad (1)$$

$$O_2^- + h^+ \rightarrow {}^1O_2 \qquad (2)$$

where e^- and h^+ are the photo-generated electron and hole pair. This is clearly different from the formation of the singlet oxygen by a collision between a dye and a triplet molecular oxygen in photo-sensitizing reaction.

In 1971, Sancier and Morrison [2] found that ESR signals due to O_2^- and lattice defect (hole traps) over UV-illuminated TiO_2 change drastically when illuminated in the presence of quinoline; i. e., the O_2^- signal is enhanced while defect signal disappears. They interpreted the phenomenon that a hole trapped on the defect is transferred to the adsorbed quinoline to form positively charged quinolone Q^+ and subsequently charge transferred complex $Q^+ - O_2^-$ is stabilized. Bickley et al. reported the similar phenomenon in the photooxidation of isopropanol over TiO_2 that oxygen photoadsorption is promoted by pre-adsorption of isobutanol on TiO_2 [3]. This shows that isopropanol is oxidized by a photoformed hole and oxygen is reduced by a photoformed electron resulting in the charge transfer via. TiO_2

photocatalyst between adsorbed oxygen and isopropanol. In this connection, Zakharenko et al. reported [4, 5] that in CO photo-oxidation over ZnO, adsorbed O_2^- is formed by illumination of light with the quantum energy lower than ZnO band gap energy while CO oxidation proceeds only under illumination of light with energy higher than band gap (band-gap-illumination). This phenomenon was also examined by Murphy et al. [6] and they concluded that CO oxidation is dominated by the hole h^+ which reacts with the lattice oxygen O_l^{2-} resulting in the formation of O_l^- expressed as follows.

$$O_l^{2-} + h^+ \rightarrow O_l^- \qquad (3)$$

The same phenomenon was observed by Teichner et al. [7] in the photo-oxidation of isobutene over TiO_2; i. e., adsorbed O_2^- is formed by illumination of the light with the energy lower than TiO_2 band gap energy while isobutane oxidation proceeds only under band-gap-illumination. Herein, the interesting points are the formation of adsorbed O_2^- radicals by illumination of the light with the lower quantum energy than band gap energy. Electrons trapped by Ti ions, reduced sites, seems excited to the conduction band and transferred to adsorbed oxygen to form O_2^-. In this case, the reduced sites behave as electron donors. Thus, the photoillumination causes the band gap excitation of semiconductor-type metal oxide as well as direct excitation between donor levels and conduction band.

Here, we would like to pay attention to the direct electron transition between the donor/acceptor level generated by adsorbed molecules and the conduction/valence band and the possibility of this electron transition for photo-illuminated semiconductor-type metal oxide is discussed. The band structure of the metal oxides determines the utilizable light energy, oxidizability, and reducing ability in their photocatalysis. Therefore, a number of studies are related to the control of band structure of metal oxide [8-11]. Many researchers have been prepared the "*pre-doped*" or "*pre-modified*" photocatalysts with metals or ions to control the band structure, in other words, utilize the visible light. For example, N-doped TiO_2

can adsorb the visible light and shows photocatalytic activity under visible light irradiation [12-16]. On the other hand, there has been no report that the effective wavelength of photo-reaction is shifted to a longer wavelength by the formation of donor/acceptor level derived from adsorbed molecule on the catalyst during a chemical reaction. Here, we shall call this type of photocatalyst modification "*in situ doping*". We demonstrate that a redshift of effective wavelength due to the direct electron transition bewteen the donor/acceptor level derived from adsorbed molecule and the conduction/valence band in the following three types of reactions; the photo-SCR on TiO_2 with NH_3 in the presence of O_2 (photo-SCR), the photo-oxidation of alcohols or imines on Nb_2O_5 with O_2, and the photo-reduction of CO_2 with H_2 or CH_4 on MgO or ZrO_2.

2. The donor level generated by adsorbed molecule

2.1. Photo-activation of adsorbed NH_3 on TiO_2: Photoassisted Selective Catalytic Reduction (photo-SCR) with NH_3

2.1.1. SCR with NH_3

NO*x* is one of the environmental pollutants and causes acid rain and photochemical smog. Therefore, it is desirable to remove NO*x* (de-NO*x*) in the stationary emission source and the mobile emission source. In the stationary emission source, NO*x* is conventionally removed from the exhaust gas by the selective catalytic reduction system with NH_3 as a reductant (NH_3-SCR) in the presence of the excess O_2 ($4NO + 4NH_3 + O_2 \rightarrow 4N_2 + 6H_2O$) over V_2O_5-based catalysts such as V_2O_5-WO_3 (or V_2O_5-MoO_3)/TiO_2 [17-20]. This system shows high NO conversion (99%), high N_2 selectivity (> 90%) and resistance for H_2O and SO*x*, although the catalyst requires high operating temperature (573−673 K) [21]. Since the NH_3-SCR system is often located downstream of the de-SO*x*, de-halogen and dust collection systems to inhibit deactivation of catalyst, the inlet temperature of the exhaust gas in the

NH_3-SCR system falls below 453 K. Consequently, it is necessary to re-heat the catalysis bed and the gas up to the operating temperature of the catalyst. Therefore, it is desired to develop a new de-NO*x* system working at low temperature (< 453 K).

Since NH_3 is quite stable, the activation of NH_3 seems to be key step in the low-temperature NH_3-SCR and SCO systems. Recently, we found that TiO_2 can activate NH_3 at low temperature and acts as an effective catalyst for both photo-SCR with NH_3 and photo-SCO [22-34]. We have clarified the activation mechanism of adsorbed NH_3 on TiO_2 and found that the direct electorn trnasfer from donor level derived form adsorbed amido (NH_2) species to the conduction band of TiO_2 was involved in the activation mechanism of adsorbed NH_3 on TiO_2.

2.1.2. Photo-SCR with NH_3 onTiO_2

Figure 1 shows the time course of N_2 evolution rate of photo-SCR. NO conversion and N_2 selectivity attained to 100 % and 96 % respectively in the conventional fixed bed flow system (GHSV = 8,000 h^{-1}). The N_2 evolution rate gradually increased at the initial stage and reached a steady rate at 1.5 h. However, when the reaction gas (a mixture of $NO/NH_3/O_2$) was passed in the dark for 0.5 h, and then photo-irradiation was started, the N_2 evolution rate immediately jumped to the level of the steady rate [23, 27]. This clearly indicates that the induction period was the time for saturation of the adsorption equilibrium of the reactant molecule. When NH_3 were passed for 1.5 h in the dark, then the gas was switched to a mixture of NO/O_2 and the photo-irradiation was started, N_2 was evolved. The N_2 evolution rate gradually decreased and the total amount of evolved N_2 was consistent with that of equilibrium adsorption of NH_3 on TiO_2. On the contrary, when a mixture of NO/O_2 was firstly passed and then switched to NH_3, neither N_2 nor N_2O was formed. These results suggest that NH_3 species adsorbed on Lewis acid site is excited by photo-irradiation and reacts with NO in the gas phase to produce N_2.

Furthermore, this is supported by the fact that only $^{15}N^{14}N$ was evolved in the photo-SCR of ^{15}NO with $^{14}NH_3$ in the presence of O_2 [24, 35].

2.1.3. Action spectrum of photo-SCR with NH_3 on TiO_2

Figure 2 shows the apparent quantum efficiency of the photo-SCR over TiO_2 as a function of the incident light (action spectrum) and a UV-Vis spectrum of TiO_2. The band gap of this TiO_2 was estimated to 3.28 eV (photo-excitation energy is 385 nm). The action spectrum is in good agreement with the UV-Vis spectrum of TiO_2 in the region of wavelength < 385 nm, where the holes and electrons generated by the bad gap excitation of TiO_2 are the driving force in the photo-SCR reaction. On the other hand, above 385 nm, the action spectrum exhibited a different behavior from that of the UV-vis spectrum. Photo-SCR proceeded under irradiation up to ca. 450 nm (2.76 eV), although the band gap of this TiO_2 was estimated to 3.28 eV. The feature of this action spectrum is analogous to the UV-Vis spectrum of N-doped TiO_2 [12, 13, 36]. It seems that the electron transfer from N 2p of adsorbed NH_3 to Ti 3d directly took place in this region. It is thought that the doping effect, such as nitrogen-doped TiO_2, would occur in the case of TiO_2 surface with adsorbed NH_3 in the photo-SCR in the wavelength region above 385 nm.

2.1.4. Photo-activation mechanism of NH_3 on TiO_2

The adsorbed species and intermediates of photo-SCR were identified by *in situ* FT/IR spectra (Fig. 3). After NH_3 adsorbed on TiO_2, the bands (1136, 1215, and 1599 cm^{-1}) due to adsorbed NH_3 species on Lewis acid site of TiO_2 appeared [37-39]. The bands at 1599 and 1215 cm^{-1} retained their intensity after evacuation (Fig. 3 (b)) and exposure to NO in the dark (Fig. 3 (c)). The intensity of the bands due to adsorbed NH_3 decreased gradually with irradiation time. On the other hand, the band at 1624 cm^{-1}, which is assignable to the

deformation vibration of H_2O [40], grew. Furthermore, new bands between 1400 and 1600 cm^{-1} were observed and then disappeared. These new bands are assigned to the nitrosamide species (NH_2NO) by comparing the FT/IR spectrum of TiO_2 exposed with ^{14}NO and NH_3 to that exposed with ^{15}NO and NH_3 [24, 35]. These results indicate that the intermediate of photo-SCR is the nitrosamide species and the nitrosamide species is decomposed to N_2 and H_2O. Moreover, it was confirmed that the Ti^{3+} species of TiO_2 reduced by H_2 was re-oxidized to the Ti^{4+} species by exposure to O_2 easily even at room temperature using UV-Vis spectroscopy [31].

Figure 4 shows the ESR spectra of TiO_2. After evacuation at 673 K, the signals are derived from the Ti^{3+} species (Fig. 4 (a)) [41-44]. There is little change in ESR signal by the exposure of NH_3 to TiO_2 in the dark. On the other hand, ESR signal changed drastically after photo-irradiation. New signals assignable to NH_2 radical [45-48] were detected together with signals assigned to Ti^{3+}. These new signals were quite stable even after more than 1 hour at 123 K without photo-irradiation. The half-life of charge-separated state of TiO_2 was estimated to be below 100 ps [49, 50]. It is widely thought that the photo-generated electrons and holes are consumed by recombination much more rapidly than by the photocatalytic reaction and the recombination is the main reason of too short lifetime of the charge-separated state and resulting in low activity of TiO_2. On the other hand, the half-life of NH_2 radical on TiO_2 at reaction temperature of photo-SCR (323 K) was calculated to be 1.4 min [31]. This suggests that the holes were trapped by NH_2 radical and recombination of the photo-generated electrons and holes was inhibited. However, these signals immediately disaapeared by the exposure to NO in the dark whereas the intensity of signals due to Ti^{3+} species increased. Based on these results, we concluded that 1) the photo-generated electron is trapped on Ti^{4+} to form Ti^{3+} and positive hole is captured by adsorbed NH_3 species to convert to active NH_2 radical, and that 2) NO in the gas phase attacks the NH_2 radical on TiO_2 rapidly. As both NH_2

radical and NO are doublet state species, it follows that NH_2 radical reacts with NO easily without irradiation. Moreover, the formation of a NH_2NO intermediate was confirmed by FT/IR spectroscopy after admittance of NO to TiO_2 adsorbing NH_3 under photo-irradiation. As described above, the intensity of signals due to Ti^{3+} species increased after the introduction of NO. It seems that the electron transfer took place from the N atom of adsorbed NH_3 to the Ti atom of TiO_2 bulk. In other words, the photo-generated electron was trapped on Ti atom and the photo-generated hole was captured by the NH_2^- species derived from adsorbed NH_3. As a result, the NH_2^- species converted to the active NH_2 radical. On the other hand, the electron may move into inside of TiO_2 bulk as a stable free electron. Before the exposure to NO, recombination took place between a part of Ti^{3+} species and the NH_2 radical. On the other hand, after the exposure to NO, the electron could not recombine because of losing an opponent (NH_2 radical). The electron was localized and stabilized in inside of TiO_2, and the signals assigned to the Ti^{3+} species increased in intensity.

On the basis of these results, we proposed Eley-Rideal type mechanism as follows (Scheme 2) [24, 27, 28, 31, 34]; 1) the NH_3 adsorbs on Lewis acid site of TiO_2, 2) the adsorbed NH_3 species is excited by photo-irradiation, 3) the excited species (NH_2 radical) reacts with NO in the gas phase to form the nitrosamide species (NH_2NO), 4) the nitrosamide species is decomposed to N_2 and H_2O, and 5) Ti^{3+} site is re-oxidized by molecular oxygen.

2.1.5. Generation of donor level derived from NH_3 adsorbed on TiO_2

Action spectrum of photo-SCR with NH_3 on TiO_2 (Fig. 2) indicates that the mechanism of the NH_2 radical formation at wavelength <385 nm is different from that at >385 nm. To reveal whether a new energy level derived from adsorbed NH_3 on TiO_2 is located between the valence band (HOMO) and the conduction band (LUMO) of TiO_2 or not, density functional theory (DFT) calculations were employed [31]. Figure 5 shows the model for dissociative

adsorption of NH_3 on the $Ti_7O_{27}H_{26}$ cluster model for the TiO_2 (101) anatase surface. The energy levels of the molecular orbitals around HOMO and LUMO for this model are shown in Fig. 6. We confirmed that occupied and virtual orbitals around HOMO and LUMO of the $Ti_7O_{27}H_{26}$ cluster (before adsorption of NH_3) consist of O 2p and Ti 3d orbitals, respectively. Figure 7 shows selected molecular orbitals. The $Ti_7O_{27}H_{26}$ model cluster with dissociative adsorbed NH_3 exhibited quite different electronic state from the $Ti_7O_{27}H_{26}$ model cluster. HOMO of the $Ti_7O_{27}H_{26}$ model cluster with dissociative adsorbed NH_3 consists of N 2p orbital of NH_2. This result clearly indicates that N 2p electron donor level is located between O 2p and Ti 3d when NH_2 species are formed on a TiO_2 surface by the dissociatively-adsorption of NH_3. Indeed, the ESR signal of NH_2 radical was obtained under visible light irradiation ($\lambda > 400$ nm, Y-43 cutoff filter used), although the ESR signal intensity was lower than under UV irradiation ($\lambda > 300$ nm). Apparently non-dissociatively adsorbed NH_3 had liittle influence the electronic states of $Ti_7O_{27}H_{26}$, for example, the molecular orbitals of HOMO, HOMO–1 and LUMO in the $Ti_7O_{27}H_{26}$ cluster closely resemble to those in the NH_3–adsorbed one. This result indicates that the electron transfer occurs from O 2p to Ti 3d regardless of the adsorption of NH_3.

Based on these results, we conclude that the photo-activation of NH_3 adsorbed on TiO_2 to NH_2 radical occurs through two paths as shown in Scheme 3. One is the electron transition from the valence band consisting of O 2p orbitals to the conduction band consisting of Ti 3d orbitals of TiO_2. This electron transition mainly takes place in the region of the wavelength <385 nm. The other is the direct electron transfer from N 2p of adsorbed NH_3 to Ti 3d. This N 2p electron donor level formed between O 2p and Ti 3d enables the photo-SCR to proceed even under visible light irradiation (400-450 nm), in other words, a lower energy than the band gap energy of TiO_2. It can be thought that the expansion of the effective wavelength of TiO_2 by adsorption of NH_3, called here, "*in situ doping*", is one of the factors for high activity

of TiO_2 in the photo-SCR.

2.2. Photo-activation of alcohols and amines on Nb_2O_5

2.2.1. Photo oxidation of alcohols and amines with molecular oxygen

Catalytic alcohol oxidation to carbonyl compounds is one of the most important chemical transformations used in the industrial chemistry and in organic syntheses [51-53]. Oxidation of amines to imines is also an important chemical transformation because of the versatile applications of imines as synthetic intermediates of medicines and biologically active nitrogen containing organic compounds [54]. Several oxidation procedures with stoichiometric, toxic, corrosive and expensive oxidants have been reported [51-58]. However, a catalytic system using molecular oxygen as a sole oxidant has been desired [55, 59-64].

In this respect, photocatalytic oxidation with molecular oxygen has been receiving noticeable attention. TiO_2 has been identified as one example of a practical and useful photocatalysts [65-68], and widely used in degradation of organic pollutants in air and water. However, in the most part of these reports, TiO_2 is used in vapor phase oxidations at high temperature, oxidation of only lower alcohols, and a low selectivity to partial oxidized products due to excess photo-activation of target products which leads to deep oxidation. Zhao et al. [69, 70] reported that the photooxidation of alcohols on TiO_2 could be dramatically accelerated without any loss of selectivity by adsorption of Brønsted acid and this effect by Brønsted acid results from the decomposition of the relatively stable side-on peroxide promoted by the protons, which effectively clean the catalytic Ti-OH_2 sites. However, this system requires the use of benzotrifluoride as a solvent. They also reported that photooxidation of amines on TiO_2 under UV irradiation gave a high selectivity to imines under a diluted conditions (e.g. 10 mg of catalyst, 0.1 mmol of amine, and 5 ml of solvent) [71]. Su and co-workers reported that mesoporous graphite carbon nitride (mpg-C_3N_4) can

work as effective photocatalysts for the selective oxidations of benzylic alcohols and amines with visible light [72, 73]. Although mpg-C_3N_4 exhibits excellent catalytic performance under visible light irradiation, high pressure of oxygen (> 0.5 MPa) and benzotrifluoride as a solvent are required to give a good yield. Shiraishi and co-workers reported that TiO_2 partially covered with WO_3 showed activity for the photooxidation of alcohols in water with molecular oxygen under irradiation at $\lambda > 350$ nm [74]. In the case of photooxidaiton of benzylalcohol, the selectivity to benzaldehyde reached at 56 % at 50% of alcohol conversion under diluted condition (5 mg of catalysts, 0.1 mmol of benzylalcohol, 5 mL of water as a solvent).

2.2.2. Photo-oxidation of alcohols and amines with molecular oxygen on Nb_2O_5

Recently, we found the photo-oxidation of alcohols to carbonyl compounds selectively proceeds over Nb_2O_5 at low temperature without organic solvents and without any additives [75-78]. Various metal oxides (SiO_2, MgO, Al_2O_3, ZrO_2, V_2O_5, Ta_2O_5, MoO_3, and WO_3) showed no activity and the activity of ZnO was very low. TiO_2 showed higher activity than Nb_2O_5, however, the Nb_2O_5 catalyst showed higher selectivity than TiO_2 at the same conversion level, indicating that Nb_2O_5 is suitable for selective oxidation. The photo-oxidation did not take place in the dark. Autooxidation proceeded when 1-phenylethanol, cyclohexanol and benzylalcohol were irradiated without catalyst. This was due to the formation of radical species by the photo-decomposition of carbonyl compounds (Norrish Type I reaction) which were present as impurities in the alcohols. Nb_2O_5 catalyst improved the conversions and/or selectivities to carbonyl compounds greatly. The less reactive primary alcohol, 1-pentanol was also photooxidized selectively by using Nb_2O_5 catalyst. The Nb_2O_5 catalyst was reusable and showed the same conversion and selectivity without any pretreatment as the catalyst as prepared.

The oxidation of various amines including primary, secondary and bicycloamine derivatives

were examined by using the Nb_2O_5 photocatalyst (Table 1) [79]. Primary benzylamine derivatives bearing various functional groups (OMe, Me, H, Cl and CF_3) were converted to corresponding coupled imines with excellent yields (entries 1–7). A primary aliphatic amine was also converted to correspoding coupled imine, but the selectivity was lower than those of benzylic homologues (entry 8). Secondary *N*-alkylbenzylamines (alkyl = Bn, Ph, *i*Pr and *t*Bu) were also oxidized to dehydrogenated imines. (entries 9–12). Relative high yields were observed in the oxidations of *N*-isopropylbenzylamine and dibenzylamine. On the other hand, *N*-phenyl and *N*-*tert*-butyl derivatives were oxidized very slowly. Benzaldehyde was formed as a by-product in the oxidations of these secondary benzylic amines. The formation of benzaldehyde is attributed to the oxidative cleavage of the C–N bond. In addition, a small amount of *N*-benzylidene benzylamine was also yielded in these cases. This represents an involvement of the C–N bond cleavage, followed by coupling of the fragments. 1,2,3,4-tetrahydroisoquinoline was smoothly converted to mono-dehydrogenated 3,4-dihidroisoquinoline with high yield (entry 13). In contrast, the rate of oxidation of 1,2,3,4-tetrahidroquinoline to aromatized quinoline was much slower than the *iso*-isomer (entry 14). In this case, a small amount of mono-dehydrogenated 3,4-dihidroquinoline as an intermediate product was also detected. The significant difference of the reaction rate between the tetrahydroquinoline isomers is generally observed in various catalytic systems [73, 80-82]. Indole was yielded with moderate selectivity in the oxidation of indoline. The Nb_2O_5 photocatalyst was reusable and showed the same conversion and selectivity of fresh catalyst without any pretreatment as well as photooxidation of alcohol. The amine oxidations over Nb_2O_5 took place even under visible light (> 390 nm) irradiation (entries 1’ –15’). Although the reaction rates were lower than that under UV (> 300 nm) irradiation, comparable selectivities were obtained. In the absence of Nb_2O_5, oxidation of benzylamine did not proceed under visible irradiation (entry 1’).

2.2.3. Action spectrum of photooxidation of alcohol on Nb_2O_5

Figure 8 shows the apparent quantum efficiency of photo-xidation of 1-pentanol as a function of the wavelength of the incident light (action spectrum) and a UV-Vis spectrum of Nb_2O_5. Nb_2O_5 exhibited an intense absorption band aroud 275 nm corresponding to the interband transition (from valence band to conduction band) of Nb_2O_5. Although band gap of Nb_2O_5 was estimated as about 3.2 eV (for a photoexcitation wavelength of 390 nm), the photo-oixdation of 1-pentanol took place under irradiation up to ca. 480 nm. A red shift of the effective wavelength is similar to that of photo-SCR over TiO_2. A slight increase in absorption around 300-350 nm was observed by adsorption of 1-pentanol on Nb_2O_5. The difference spectrum before and after the absorption of 1-penatnol showed an absorption band at 340 nm. It is reported that 1-pentanol had no absorption at wavelength longer than 300 nm. Therefore, this band around 340 nm would be attributed to absorption of a surface complex consisting of adsorbed alcohol and Nb_2O_5. The action spectrum of the photo-oxidation of 1-pentanol on Nb_2O_5 showed a good correlation with the difference spectrum, suggesting that the photo-oxidation of alcohol was triggered by light absorption of the surface complex consisting of adsorbed alcohol and Nb_2O_5.

A red shift of the effective wavelength was also observed in the photo-oxidation of benzylamine over Nb_2O_5 [79]. The photo-oixdation of benzylamine took place under irradiation up to ca. 460 nm. The difference spectrum before and after the absorption of benzylamine showed an absorption band at 350 nm. Since benzylamine has no absorption at wavelength longer than 300 nm, this band around 350 nm would be attributed to absorption of a surface complex consisting of adsorbed amine and Nb_2O_5. This result strongly suggests that the photo-oxidation of amine was also triggered by light absorption of the surface complex consisting of adsorbed amine and Nb_2O_5.

2.2.4. Mechanism of photo-oxidation of alcohols on Nb_2O_5

The adsorbed species and intermediates of photo-oxidation were identified by *in situ* FT/IR spectra of adsorbed cyclohexanol on Nb_2O_5. Figure 9 shows the FT/IR spectra of adsorbed cyclohexanol on Nb_2O_5. The bands at 1467 and 1452 cm^{-1} were assigned to $\delta_s(CH_2)$ and the bands at 1363 and 1347 cm^{-1} were assigned to $\omega(CH_2)$, respectively. The new bands at 1091 and 1126 cm^{-1} appeared after the adsorption of cyclohexanol on Nb_2O_5. These bands are assigned to the stretching mode of a C-O bond in the alkoxide species on the Nb_2O_5, because the formation of the alkoxide species by the adsorption of alcohol is usually accompanied by a shift of the stretching mode of a C-O bond to a higher wavenumber [83-85]. Under UV irradiation (< 390 nm), the intensity of the band assigned to ν(C-O) (around 1090 cm^{-1}) decreased as the irradiation time increased, whereas the bands assigned to ν(C=O) (1676 cm^{-1}) and the symmetric-stretching of the carboxylic acid anion (1554 cm^{-1}) gradually grew. This result indicates that the alkoxide species on Nb_2O_5 was excited by photons and oxidized to carbonyl compounds. The carbonyl compounds were formed even under visible light irradiation (> 390 nm).

A broad ESR signal around g = 1.9 was observed at 123 K, when 1-pentanol was adsorbed on Nb_2O_5 under UV-irradiation. This broad signal at g = 1.9 was assignable to Nb^{4+} [86, 87] and immediately disappeared by the exposure to O_2 in the dark, indicating that Nb^{4+} was oxidized to Nb^{5+} rapidly even at 123 K. On the other hand, when 1-pentanol was adsorbed on Nb_2O_5 under UV-irradiation at 77K, ESR signal (g = 2.006, A_{H1} = 2.0 mT, A_{H2} = 4.4 mT) assigned to alkoxide carbon radical species was observed. These new signals were stable at 77 K without photo-irradiation, but disappeared at room temperature. The signal did not change in the presence of O_2 even under UV-irradiation, indicating that the alkoxide carbon radical species dose not react with O_2.

On the basis of these results, we proposed the reaction mechanism of photo-oxidation of alcohol on Nb_2O_5 (Scheme 4) [75-77]; 1) alcohol is adsorbed on Nb_2O_5 to form alkoxide species, 2) the photo-formed electron is trapped on Nb^{5+} to form Nb^{4+} and positive hole is captured by alkoxide species to convert to active alkoxide carbon radical, 3) the active alkoxide carbon radical is dehydrogenatied to carbonyl compound (the reduction of Nb^{5+} to Nb^{4+} takes place simultaneously), 4) the product desorbs, and 5) the reduced Nb^{4+} sites are re-oxidized by the reaction with O_2.

2.2.5. Generation of donor level derived from alcohol and amine adsorbed on Nb_2O_5

In order to investigate the formation of a new energy level derived form adsorbed alcohol, DFT calculations were employed. The electronic structure of the model of alkoxide-Nb_2O_5 complex was compared to that of Nb_2O_5 by DFT calculations. Figure 11A shows the model cluster of the T-phase Nb_2O_5 (**1**; $Nb_{12}O_{43}H_{26}$) and that of dissociative adsorption of methanol onto T-phase Nb_2O_5 (100) surface (**2**; $Nb_{12}O_{42}H_{25}(OCH_3)$). In the cluster **2**, one terminal hydroxyl group was substituted with methoxy one. The occupied and the virtual orbitals of these model clusters consisted of O 2p orbitals and Nb 4d orbitals, respectively. Figure 11B shows selected frontier orbitals of **1** and **2**. The cluster **2** exhibits quite different electronic state from the cluster **1**. Particularly with HOMO and HOMO–1 of **2**, O 2p orbitals localize on oxygen atom of the methoxy group. The energy levels of HOMO and HOMO–1 are higher than that of HOMO of **1**, whereas the energy levels of LUMO and other unoccupied orbitals of **1** and **2** are almost same (Fig. 12). These results clearly showed that donor levels whose populations are localized on the alkoxide oxygen were generated between the HOMO and LUMO levels of Nb_2O_5 by the formation of surface complex (alkoxide-Nb_2O_5) and that the electron transitions from O 2p donor level derived from the adsorbed alkoxide species to the conduction band of Nb_2O_5 (Nb 4d orbitals) had lower energy than those from O 2p of Nb_2O_5

(the conduction band) to Nb 4d [77]. Indeed, the electron excitation energies of **1** and **2** calculated by TD-DFT (time dependent-DFT) revealed that lower energy transition takes place with **2** than with **1**. Thus, the photo-oxidation of alcohols proceeding by lower-energy light than the band gap of Nb_2O_5 can be explained by excitation of the surface complex, i.e., direct electron excitation from O 2p orbital localized on alkoxide oxygen to conduction band of Nb_2O_5 consisting of Nb 4d orbital (Scheme 5).

On the basis of these results, we concluded that the photo-oxidation of alcohol over Nb_2O_5 takes place through the direct electron transfer from the O 2p orbital of adsorbed alkoxide species to the conduction band consisting of Nb 4d orbitals ("*in situ doping"*). As a result of "*in situ doping"*, the photo-oxidation of alcohol proceeded even under visible light irraidiation. In a analogous way, amine oxidation over Nb_2O_5 with visible light may be attributed to a direct electron transfer from a donor level consisting of a N2p orbital derived from adsorbed amide species (Scheme 6) [79]. At first, dissociative adsorption of amine forms an amide (RR'N-Nb) species. The photo-formed electron is trapped on Nb^{5+} to form Nb^{4+} and positive hole is captured by amide species to convert to active amide radical. The active amide radical is dehydrogenated to imine compound. Then, photo-formed imine desorbed from Nb_2O_5. Finally, the reduced Nb^{4+} sites are re-oxidized by the reaction with O_2. The corresponding primary imine was not detected. However, ammonia and benzaldehyde in addition to *N*-benzylidene benzylamine were detected, indicating that the hydrolysis of primary imine took place. Moreover, when benzaldehyde was added to benzylamine in the absence of Nb_2O_5 under the dark, the condensation of benzaldehyde and benzylamine to *N*-benzylidene benzylamine immediately and quantitatively proceeded. These results indicate that a rapid dimerization takes place regardless of catalyst and photo-irradiation; the produced primary imine is hydrolyzed to aldehyde and ammonia, followed by condensation of the aldehyde and the primary amine.

3. Acceptor level generated by adsorbed molecule

3.1. Chemical fixation and photocatalytic reduction of carbon dioxide

Carbon dioxide (CO_2) is regarded as one of the greenhouse effects gases, that cause the global warming by absorption of the infrared ray and enclose it in air [88]. The relationship between the emission of CO_2 is still under discussions, however, it is certain that the emission of CO_2 should be reduced [89]. Up to now, a number of different ways for the reducing of CO_2 emission including strage in the ground and sea, absorption into various functionalized materials, and large scale forestation has been proposed. On the other hand, the transformation of CO_2 to harmless and/or valuable chemicals seems to be quite attractive way for the reducing of CO_2 emission. However, this is one of the important challenges in chemistry because CO_2 is remarkably stable. Therefore, severe reaction conditions of high pressure and/or high temperature are often required.

On the other hand, in photocatalytic reactions the reaction system in the initial stage is activated to have an additional chemical potential by photoirraidiation. Therefore, photocatalysts often permit the reaction which hardly proceeds under the usual condition. There are manu studies that have tried to reduce CO_2 under irradiation using several photocatalysts [90-98]. We found that Rh/TiO_2, MgO, ZrO_2 and Ga_2O_3 enable the reduction of CO_2 to proceed at room temperature and ambient pressure [99-108]. Here, the detail of the photoreduction of CO_2 over MgO and ZrO_2 is described in the following sections.

3.2. Photoreduction of CO_2 on MgO

3.2.1. Photoreduciton of CO_2 with H_2 or CH_4 on MgO

MgO exhibited photocatalytic activity for the reduction of CO_2 to CO using H_2 or CH_4 as a reductant [106, 107]. After 5 h of photoirradiation using CH_4 as a reductant, the amount of

evolved CO reached 3.6 μmol. After 6 h of photoirradiation using H_2, the CO evolution was 2.9μmol. When the reaction was carried out in the dark, without a catalyst or without a reductant (H_2 or CH_4), no CO was detected, indicating that 1) photo-reduction of CO_2 on MgO was due entirely to a photocatalytic reaction, and that 2) H_2 and CH_4 were required as a reductant of CO_2. Only a small amount of CO was formed on MgO by irradiation with a wavelength longer than 290 nm. This indicates that the reaction requires UV light with a wavelength shorter than 290 nm. Since the light source (a 500 W ultrahigh-pressure mercury lamp) does not supply light with sufficient energy to excite the intrinsic band gap of MgO, the intrinsic band gap excitation of MgO is not essential in this photoreaction. This fact strongly suggests that electron transfer between MgO and CO_2 is important in this photoreaction.

Figure 13 shows change in the amount of CO evolution and CH_4 consumption over MgO under photoirradiation. The amount of consumed CH_4 was considerably larger than that of evolved CO up to 8 h of reaction. The amount of consumed CH_4 was not compatible with the CO evolution stoichiometrically. This suggests that intermediate anchored on the surface of MgO during the photo-reducition of CO_2.

3.2.2. Surface species on MgO

Figure 14 shows the dependence of the initial amount of introduced CO_2 on the amount of CO evolved from the photocatalytic reduction and subsequent heat treatment using CH_4 as a reductant. No CO evolution from the photocatalytic reaction was detected until the amount of introduced CO_2 reached 66 μmol•g-MgO^{-1}. The CO evolution increased with increasing the amount of CO_2 and then was almost constant above 133 μmol•g-MgO^{-1}, that was consistent with the maximaum amount of chmisorbed CO_2 on MgO (130 μmol•g-MgO^{-1}). On the other hand, the largest CO evolution due to heat treatment after the photocatalytic reaction was obsserved when the amount of introduced CO_2 was 66 μmol•g-MgO^{-1}. When the introduction

of CO_2 was larger than 133 μmol•g-MgO^{-1}, the amount of CO_2 had a little influence on the amount of the CO evolution due to heat treatment. The amount of chemisorbed CO_2 was compatible with the minimum amount of introduced CO_2 in yielding the maximum CO evolution due to the photocatalytic reaction (133 μmol•g-MgO^{-1}). The introduction of 66 μmol•g-MgO^{-1} of CO_2 caused the largest CO evolution by heat treatment. In addition, the CO evolution due to the photocatalytic reaction could be detected in the gas phase after the amount of introduced CO_2 reached 66 μmol•g-MgO^{-1}. The CO evolutions due to the photocatalytic reaction and heat treatment were constant after the amount of introduced CO_2 reached 133 μmol•g-MgO^{-1}. Interestingly, there were two different thresholds in the photocatalytic reduction of CO_2 over MgO. These results suggest that the species produced when the introduced CO_2 is below 66 μmol•g-MgO^{-1} is different from that produced when it is larger than 66 μmol•g-MgO^{-1}. The similar effect of the initial amount of introduced CO_2 on the amount of CO evolved using H_2 intead of CH_4 [106].

Figures 15 and 16 represent the IR spectra of adsrbed species on MgO (a) after exposure to CO_2 and evacuation, (b) after exposure to CO_2 and H_2 or CH_4 and photoirraidiation, and (c) after evacuation. When MgO was exposure to CO_2, many bands appeared in the region of 1800-2500 cm^{-1} because of the formation of several caronate species (unidentate, bidentate, and bicarbonate) [83] [109-111]. We investigated the effect of the amount of introduced CO_2 on the intensity of bands due to two bidentate carbonates (Fig. 17). Both species were detected when a small amount of CO_2 was introduced. Yanagisawa et al. reported that the bands due to species A increased in intensity at 373 K, whereas the bands due to species B disppeaed [111], indicating that species A adsorbed strongly on MgO than species B. The increase in the absorbance of the bands at 1660 and 1310 cm^{-1} due to species A stopped after the introduced CO_2 exceeded 66 μmol g-MgO^{-1}. On the other hand, the band at 1624 cm^{-1} due to species B increased when a sufficient amount of CO_2 (>66 μmol g-MgO^{-1}) was introduced.

Based on these resluts combined with the effect of amount of CO_2 on the CO formation, it is conluded that species A, was reduced to a mere intermediate that was inactive for CO evolution. Above 66 μmol•g-MgO^{-1} of CO_2, species B was generated instead of species A. It seems that species B was reduced to a surface-active intermediate that can react with H_2 or CH_4 to produce CO from CO_2.

Figures 15(b) and 16(b) show the IR spectra of MgO after irradiation in the presence of H_2 or CH_4. Increase or decrease in intensity and appearance of new bands were observed in the IR spectra in the region of 2900-2700 and 1800-1250 cm^{-1}. New bands at 2957, 2830, and 2730 cm^{-1} assigned to a C-H stretching vibration band [112, 113] appeared (the inset in Fig. 6). Since surface carbonates have no C-H stretching vibration mode, the appearance of these bands exhibits the formation of a surface species containing a C-H bond. The difference IR spectrum of MgO irradiated in the presence of H_2 was similar to that of formaldehyde species adsorbed on MgO [114]. Therefore, it was concluded that the surface species arising during the photoreaction between CO_2 and H_2 is a surface bidentate formate. On the other hand, the inset in Fig. 16 shows the subtraction of the IR spectrum of adsorbed species on MgO in the presence of CH_4 before photoirradiation (Fig. 16(a)) from that after photoirradiation (Fig. 16(b)). In the case of using CH_4 as a reductant, new bands in the region of 2900-2700 and 1800-1250 cm^{-1} were observed in addition to the bands due to bidentate formate. These new bands were assaignable to an acetate. Consequently, the species adsorbed on MgO converts to the surface bidentate acetate as well as the surface bidentate formate as an intermediate in the presence of CH_4 under photoirradiation.

3.2.3. Reactivity of Surface species on MgO

To investigate the role of the surface bidentate formate and the surface bidentate acetate as an intermediate, we carried out the CO_2 photocatalytic reduction over MgO pretreated with

HCHO or CH_3CHO. When HCHO or CH_3CHO solely was introduced onto MgO, no CO was detected even after photoirradiation. CO was not observed when MgO was irradiated in the presence of HCHO in the presence of H_2 or CH_4. Moreover, CO was not observed when MgO was irradiated in the presence of HCHO or CH_3CHO in the presence of CH_4. However, CO was evolved when CO_2 was introduced to MgO together with HCHO or CH_3CHO under photoirradiation. This reaction did not proceed in the dark. These results indicate that the surface formate or acetate species gives CO in the presence of CO_2 under photoirradiation.

^{13}CO was formed when $^{13}CO_2$ and $^{12}CH_4$ were used as reactants, whereas ^{12}CO was formed when $^{12}CO_2$ and $^{13}CH_4$ were used. This indicates that CO was derived from CO_2. The carbon atom of CO_2 was labeled by ^{13}C and the photoreaction between $^{13}CO_2$ and $H^{12}CHO$ was carried out. In this case, only ^{13}CO was formed. Therefore, CO generated was derived from CO_2. Therefore, the surface formate does not decompose to yield CO directly, but acts as a reductant and converts another CO_2 molecule to gaseous CO under photoirradiation.

These results are summarized as follows. Both the bidentate carbonates (species A and B) were generated when CO_2 adsorbed on MgO. The formation of species A took place preferentially until the amount of introduced CO_2 reachedμmol•g-MgO^{-1}. And then, species B was formed and CO was produced in the gas phase. The CO evolution by the photocatalytic reaction and the heat treatment became constant when the amount of introduced CO_2 exceeded the maximaum amount of chmisorbed CO_2 on MgO (130 μmol•g-MgO^{-1}). In conclusion, species A would be connected with only magnesium cation and remain on MgO as an inactive species because there are excessive base sites of MgO. On the other hand, species B, which was adsorbed by the side-on adsorption-type form, is reduced to a surface bidentate formate or a surface bidentate acetate by H_2 or CH_4. CO does not generate from these species. However, these species act as photoactive species on MgO.

3.2.4. Photo-activation of CO_2 on MgO

Surface bidentate formate or a surface bidentate acetate contributed to the evolution of CO under photoirradiation. Since CO_2 species adsorbed on MgO was reduced to a surface bidentate formate or a surface bidentate acetate in the presence of H_2 or CH_4. Therefore, it is expected that the CO_2 adsorbed on MgO would be photoactivated under photoirradiation. Figure 18 shows photoluminescence excitation spectra of MgO. The maximum excitation intensity appeared at 240 nm (5.2 eV), was assigned to excitation of bulk MgO. The photoluminescence excitation spectra at 240 nm was remarkably quenched by the introduction of CO_2 to MgO, indicating that CO_2 interacted with the extrinsic lattice defects. On the other hand, the intensity of the excitation wavelength at 320 nm increased when CO_2 was adsorbed on MgO. These results indicate that there are the two types of photo-excitation processes. One is due to the intrinsic band gap excitation of MgO. It can be thought that the other is due to the direct electron transfer from a new level generated between the HOMO (the valence band) and LUMO (the conduction band) levels of MgO by the formation of surface complex (bidentate carbonate-MgO) to LUMO or from HOMO to a new level. Figure shows phosphorescence emmision spectra of MgO adsorbed CO_2. The braod band observed ap at 350-600 nm was quenched by the introduction of H_2 or CH_4. This indicates that the photoactive species derived from the adsorbed CO_2 interacted with H_2 and CH_4.

EPR signals of CO_2^- and CO_3^- radicals as photoactivated species on MgO were clearly observed after the photoirradiation of MgO adsorbed MgO. These signals were highly stable in the dark after photoirradiation. However, the photoactivated species on MgO (CO_2^- and CO_3^- radicals) reacted with H_2 or CH_4. When H_2 was introduced to MgO in the dark, the signals derived from the CO_2^- and CO_3^- radicals disappeared in short order. In addition, the CO_2^- radical species vanished more quickly than the CO_3^- radical species. We concluded that in this reaction, the CO_2^- radical is reduced by H_2 to formate or acetate rather than the CO_3^-

radical.

3.2.5. Mechanism of photo-reduction of CO_2 on MgO

Based on above rsults, we propose the follwing mechanism of the CO_2 photocatalytic reduction in the presence of H_2 or CH_4 as a reductant (Scheme 7); Two bidentate carbonates (species A and B) are generated on MgO in introducing CO_2. The bidentate carbonates are activated under photoirradiation and are converted to a CO^{2-} or CO^{3-} radical. Anion species (CO^{2-} and CO^{3-} radical) was generated by the irradiation with a wavelength longer than 290 nm, indicating that the intrinsic band gap excitation of MgO is not essential in this photoactivation step. Therefore, it seems that the direct electron transfer from HOMO to a new level generated between the HOMO (the valence band) and LUMO (the conduction band) levels of MgO by the formation of surface complex (bidentate carbonate-MgO). In this case, a new level derived from surface complex (bidentate carbonate-MgO) acts as “an acceptor level” (Scheme 8). The CO^{3-} radical derived from species A was transformed to a bicarbonate, which is inactive for the CO_2 photocatalytic reduction. On the other hand, the CO^{2-} radical species derived from species B is reduced to a surface bidentate formate or acetate in the presence of H_2 or CH_4. The surface bidentate formate and acetate are highly stable on MgO and reduce CO_2 in the gas phase to CO under photoirradiation.

3.3. Photoreduction of CO_2 on ZrO_2

ZrO_2 was found to exhibit activity for the photoreduction of CO_2 with H_2 or CH_4 [101-105]. We repored that the mechanism of photoreduction of CO_2 on ZrO_2 is essentailly same to that on MgO. Bidentate carbonate was formed on ZrO_2 by the introduction CO_2. Adsorbed CO_2 (bidentate carbonate) was photoexcited to a triplet state; a part of the CO_2 in the triplet state is deactivated and returns to the ground state upon releasing an emission at 440 nm, while the

rest is stabilized as a CO^{2-} anion radical. The wavelength of light effective for the photoreduction of CO_2 was longrt than that at which ZrO_2 absorbs (< 250 nm). Therefore, the intrinsic band gap excitation of ZrO_2 is not essential in this photoactivation step and a new level generated between the HOMO and LUMO levels of ZrO_2 by the formation of surface complex (bidentate carbonate-ZrO_2). In this case, a new level acts as "an acceptor level" as well as the photoreduction of CO_2 on MgO. The CO^{2-} anion radical reacts with H_2 in the gas phase to produce the surface formate spiceis. And then, the surface formate reduces CO_2 in the gas phase to CO under photoirradiation.

4. Coclusions

The direct electron transition between the donor/acceptor level generated by adsorbed molecules and the conduction/valence band for photo-illuminated semiconductor type metal oxide ("*in situ doping*") is demonstrated.

In the case of photo-SCR over TiO_2, a new donor level from adsorbed NH_2 species was generated between the valence band (O 2p) and the conduction band (Ti 3d) by the adsorption of NH_3 on TiO_2. The direct electron transition from donor level to the conduction band took place to form NH_2 radical species by visible light irradiation and NO in the gas phase attacked the NH_2 radical to form NH_2NO (nitrosamide) intermediate (Eley-Rideal type mechanism). And then, the NH_2NO species is decomposed to N_2 and H_2O. As a result, the photo-SCR proceeded even under visible light irradiation.

Photo-oxidation of alcohols and amines with molecular oxygen selectively proceeds on Nb_2O_5. As well as the adsorbed NH_3 on TiO_2, a new electron donor level was generated between the valence band (O 2p) and the conduction band (Nb 4d) by the adsorption of alcohol or amine on Nb_2O_5. The direct electron transition from donor level derived from

alkoxide species to the conduction band took place to form alkyl carbon radical species by photo-irradiation. Therefore, the photo-formed electron is trapped on Nb^{5+} to form Nb^{4+} and positive hole is captured by alkoxide species on Nb_2O_5 to convert to alkyl carbon radical. The formed alkyl carbon radical was immediately dehydrogenated to carbonyl compound. In the case of the photo-oxidation of amines, in an analogous way, the direct electron transition from donor level derived from amide species to the conduction band took place to form amide radical species by photo-irradiation.

On the orher hand, in the cases of the photo-reduction of CO_2 to CO on MgO or ZrO_2, a new electron acceptor level was generated between the valence band and the conduction band by the adsorption of CO_2 on MgO or ZrO_2. Both MgO and ZrO_2 exhibit photocatalytic activity for the reduction of CO_2 to CO using H_2 or CH_4 as a reductant. Surface bidentate formate or surface bidentate acetate contributed to the evolution of CO under photoirradiation. The bidentate carbonates are activated under photoirradiation and are converted to a CO^{2-} or CO^{3-} radical. Anion species (CO^{2-} and CO^{3-} radical) was generated by the irradiation with a wavelength longer than 290 nm, which implies that the intrinsic band gap excitation of MgO is not essential in this photoactivation step. The direct electron transfer from HOMO to a new level generated between the valence band and the conduction band levels of MgO by the formation of surface complex (bidentate carbonate-MgO). In this case, a new level derived from surface complex acts as “an acceptor level”.

As mentioned above, the direct electron transition between the donor/acceptor level generated by adsorbed molecules and the conduction/valence band for photo-illuminated semiconductor-type metal oxide (“*in situ doping*“) resulsts in a redshift of effective wavelength and “*in situ doping*“ gives us attractive ways for the removing the limit of band gap energy, and the utilization of visible light.

Acknowledgements

This study was partially supported by and Grants-in-Aid for Scientific Research on Priority Area (No. 10734036, “Molecular Nano Dynamics” and No. 20037038, “Chemistry of Concerto Catalysis), and Scientific Research (B) (No. 19360365). K. T. was supported by the Program for Improvement of Research Environment for Young Researchers from Special Coordination Funds for Promoting Science and Technology (SCF) commissioned by the MEXT of Japan. The authors thank Dr. Yoshiumi Kohno, Dr. Seiji Yamazoe, Mr. Tai Ohuchi, Mr. Toshiaki Miyatake, Mr. Shinya Furukawa, Miss. Ayaka Tamura, and Mr. Yasuhiro Ohno at Kyoto University for the collaboration to this study.

References

[1] M.A. Fox, C.C. Chen, J. Am. Chem. Soc. 103 (1981) 6757-6759.
[2] K.M. Sancier, S.R. Morrison, Surf. Sci. 83 (1979) 29-44.
[3] R.I. Bickley, G. Munuera, F.S. Stone, J. Catal. 31 (1973) 398-407.
[4] V.S. Zakharenko, A.E. Cherkashin, N.P. Keier, G.F. Gerasimova, Kinet. Catal. 16 (1975) 142-148.
[5] V.S. Zakharenko, A.E. Cherkashin, N.P. Keier, S.V. Koshcheev, Kinet. Catal. 16 (1975) 149-154.
[6] W.R. Murphy, T.F. Veerkamp, T.W. Leland, J. Catal. 43 (1976) 304-321.
[7] M. Formenti, F. Juillet, Meriaude.P, S.J. Teichner, Bulletin De La Societe Chimique De France (1972) 69-&.
[8] K. Maeda, K. Domen, J. Phys. Chem. C. 111 (2007) 7851-7861.
[9] K. Maeda, K. Domen, Chem. Mater.. 22 (2010) 612-623.
[10] R. Abe, M. Higashi, K. Domen, ChemSusChem. 4 (2011) 228-237.
[11] A. Kudo, Y. Miseki, Chem. Soc. Rev. 38 (2009) 253-278.
[12] S. Sato, Chem. Phys. Lett. 123 (1986) 126-128.
[13] R. Asahi, T. Morikawa, T. Ohwaki, K. Aoki, Y. Taga, Science. 293 (2001) 269-271.
[14] H.M. Luo, T. Takata, Y.G. Lee, J.F. Zhao, K. Domen, Y.S. Yan, Chem. Mater.. 16 (2004) 846-849.
[15] M. Miyauchi, A.K. Nakajima, T. Watanabe, K. Hashimoto, Chem. Mater.. 14 (2002) 4714-4720.
[16] H. Yu, H. Irie, Y. Shimodaira, Y. Hosogi, Y. Kuroda, M. Miyauchi, K. Hashimoto, J. Phys. Chem. C. 114 (2010) 16481-16487.
[17] S. Cho, Chem. Eng. Prog. 90 (1994) 39-45.
[18] P. Forzatti, L. Lietti, HETEROGEN CHEM REV. 3 (1996) 33-51.
[19] F. Nakajima, Syokubai. 32 (1990) 236.
[20] S. Wood, Chem. Eng. Prog. 90 (1994) 32-38.
[21] V. Parvulescu, P. Grange, B. Delmon, Catal. Today. 46 (1998) 233-316.
[22] T. Tanaka, K. Teramura, T. Funabiki, Phys. Chem. Chem. Phys. 2 (2000) 2681-2682.
[23] T. Tanaka, K. Teramura, K. Arakaki, T. Funabiki, Chem. Commun. (2002) 2742-2743.
[24] K. Teramura, T. Tanaka, T. Funabiki, Langmuir. 19 (2003) 1209-1214.
[25] K. Teramura, T. Tanaka, T. Funabiki, Chem. Lett. 32 (2003) 1184-1185.
[26] K. Teramura, T. Tanaka, M. Kani, T. Hosokawa, T. Funabiki, J. Mol. Catal. A-Chem. 208 (2004) 299-305.
[27] K. Teramura, T. Tanaka, S. Yamazoe, K. Arakaki, T. Funabiki, Appl. Catal. B-Environ. 53 (2004) 29-36.
[28] S. Yamazoe, T. Okumura, K. Teramura, T. Tanaka, Catal. Today. 111 (2006) 266-270.
[29] S. Yamazoe, T. Okumura, Y. Hitomi, T. Shishido, T. Tanaka, J. Phys. Chem. C. 111 (2007) 11077-11085.
[30] S. Yamazoe, T. Okumura, T. Tanaka, Catal. Today. 120 (2007) 220-225.
[31] S. Yamazoe, K. Teramura, Y. Hitomi, T. Shishido, T. Tanaka, J. Phys. Chem. C. 111 (2007) 14189-14197.
[32] S. Yamazoe, Y. Hitomi, T. Shishido, T. Tanaka, Appl. Catal. B-Environ. 82 (2008) 67-76.
[33] S. Yamazoe, Y. Hitomi, T. Shishido, T. Tanaka, J. Phys. Chem. C. 112 (2008) 6869-6879.
[34] S. Yamazoe, Y. Masutani, K. Teramura, Y. Hitomi, T. Shishido, T. Tanaka, Appl. Catal. B-Environ. 83 (2008) 123-130.
[35] T. Tanaka, K. Teramura, T. Yamamoto, S. Takenaka, S. Yoshida, T. Funabiki, J. Photoch. Photobio. A. 148 (2002) 277-281.
[36] R. Asahi, T. Morikawa, Y. Taga, Abstr. Pap. Am. Chem. Soc. 222 (2001) U633-U633.

[37] G. Ramis, L. Yi, G. Busca, M. Turco, E. Kotur, R.J. Willey, J. Catal. 157 (1995) 523-535.
[38] M.C. Kung, H.H. Kung, Catal. Rev.-Sci. Eng. 27 (1985) 425-460.
[39] C.C. Chuang, J.S. Shiu, J.L. Lin, Phys. Chem. Chem. Phys. 2 (2000) 2629-2633.
[40] E. Ito, Y.J. Mergler, B.E. Nieuwenhuys, H.P.A. Calis, H. vanBekkum, C.M. vandenBleek, J. Chem. Soc.-Faraday Trans. 92 (1996) 1799-1806.
[41] P. Meriaudeau, M. Che, C.K. Jorgensen, Chem. Phys. Lett. 5 (1970) 131-133.
[42] C. Hauser, Z. Angew. Math. Phys. 22 (1971) 783.
[43] R.F. Howe, M. Gratzel, J. Phys. Chem. 89 (1985) 4495-4499.
[44] D.C. Hurum, A.G. Agrios, K.A. Gray, T. Rajh, M.C. Thurnauer, J. Phys. Chem. B. 107 (2003) 4545-4549.
[45] S.N. Foner, E.L. Cochran, V.A. Bowers, C.K. Jen, Phys. Rev. Lett. 1 (1958) 91-94.
[46] E.F. Vansant, J.H. Lunsford, J. Phys. Chem. 76 (1972) 2716-&.
[47] S. Nagai, Bull. Chem. Soc. Jpn. 46 (1973) 1144-1148.
[48] N. Shimamoto, K. Hatano, T. Katsu, Y. Fujita, Bull. Chem. Soc. Jpn. 48 (1975) 18-21.
[49] S. Ikeda, N. Sugiyama, B. Pal, G. Marci, L. Palmisano, H. Noguchi, K. Uosaki, B. Ohtani, Phys. Chem. Chem. Phys. 3 (2001) 267-273.
[50] S. Ikeda, N. Sugiyama, S. Murakami, H. Kominami, Y. Kera, H. Noguchi, K. Uosaki, T. Torimoto, B. Ohtani, Phys. Chem. Chem. Phys. 5 (2003) 778-783.
[51] R.A. Rheldon, J.K. Kochi, Metal-Catalyzed Oxidations of Organic Compounds (Academic Press, New York, 1981).
[52] M. Hudlicky, Oxidations in Organic Chemistry (American Chemical Society, Washington DC, 1990).
[53] C.L. Hill, Advances in Oxygenated Process (JAI, London, 1998).
[54] S.I. Murahashi, Angew. Chem. Int. Ed. 34 (1995) 2443-2465.
[55] R.C. Larock, Comprehensive Organic Transformations (VCH, New York, 1989).
[56] K.C. Nicolaou, C.J.N. Mathison, T. Montagnon, Angew. Chem.-Int. Edit. 42 (2003) 4077-4082.
[57] K.C. Nicolaou, C.J.N. Mathison, T. Montagnon, J. Am. Chem. Soc. 126 (2004) 5192-5201.
[58] T. Mukaiyama, A. Kawana, Y. Fukuda, J. Matsuo, Chem. Lett. (2001) 390-391.
[59] R.A. Sheldon, I. Arends, A. Dijksman, Catal. Today. 57 (2000) 157-166.
[60] T. Mallat, A. Baiker, Chem. Rev. 104 (2004) 3037-3058.
[61] K. Yamaguchi, N. Mizuno, Angew. Chem.-Int. Edit. 41 (2002) 4538-+.
[62] K. Yamaguchi, K. Mori, T. Mizugaki, K. Ebitani, K. Kaneda, J. Am. Chem. Soc. 122 (2000) 7144-7145.
[63] K. Yamaguchi, N. Mizuno, Angew. Chem.-Int. Edit. 42 (2003) 1480-1483.
[64] K. Mori, K. Yamaguchi, T. Mizugaki, K. Ebitani, K. Kaneda, Chem. Commun. (2001) 461-462.
[65] U.R. Pillai, E. Sahle-Demessie, J. Catal. 211 (2002) 434-444.
[66] J. Chen, D.F. Ollis, W.H. Rulkens, H. Bruning, Water Research. 33 (1999) 661-668.
[67] J.L. Falconer, K.A. Magrini-Bair, J. Catal. 179 (1998) 171-178.
[68] D.S. Muggli, K.H. Lowery, J.L. Falconer, J. Catal. 180 (1998) 111-122.
[69] Q. Wang, M. Zhang, C. C., W. Ma, J. Zhao, Angew. Chem. Int. Ed. 49 (2010) 7976-7979.
[70] M. Zhang, Q. Wang, C. Chen, Z. L., W. Ma, J. Zhao, Angew. Chem. Int. Ed. 48 (2010) 6081-6084.
[71] X. Lang, H. Ji, C. Chen, W. Ma, J. Zhao, Angew. Chem. Int. Ed. 50 (2011) 3934-3937.
[72] F. Su, S.C. Mathew, G. Lipner, X. Fu, M. Antonietti, S. Blechert, X. Wang, J. Am. Chem. Soc. 132 (2010) 16299-16301.
[73] F. Su, S.C. Mathew, L. Moehlmann, M. Antonietti, X. Wang, S. Blechert, Angew. Chem.-Int. Edit. 50 (2011) 657-660.
[74] D. Tsukamoto, M. Ikeda, Y. Shiraishi, T. Hara, N. Ichikuni, S. Tanaka, T. Hirai, Chem.-Eur. J. 17 (2011) 9816-9824.
[75] T. Ohuchi, T. Miyatake, Y. Hitomi, T. Tanaka, Catal. Today. 120 (2007) 233-239.

[76] T. Shishido, T. Miyatake, K. Teramura, Y. Hitomi, H. Yamashita, T. Tanaka, J. Phys. Chem. C. 113 (2009) 18713-18718.
[77] S. Furukawa, Y. Ohno, T. Shishido, K. Teramura, T. Tanaka, ChemPhysChem in press.
[78] S. Furukawa, A. Tamura, T. Shishido, K. Teramura, T. Tanaka, Appl. Catal. B-Environ. in press.
[79] S. Furukawa, Y. Ohno, T. Shishido, K. Teramura, T. Tanaka, ACS Catalysis in press.
[80] S.-I. Murahashi, Y. Okano, H. Sato, T. Nakae, N. Komiya, Synlett (2007) 1675-1678.
[81] M.-H. So, Y. Liu, C.-M. Ho, C.-M. Che, Chem. Asian Journal. 4 (2009) 1551-1561.
[82] Y. Maeda, T. Nishimura, S. Uemura, Bull. Chem. Soc. Jpn. 76 (2003) 2399-2403.
[83] L.H. Little, A.V. Kiselev, V.I. Lygin, Infrared Spectra of Adsorbed Species (Academic Press Inc., London, 1966).
[84] G. Socrates, Infrared Characteristic Group Frequencies: Table and Charts (Wiley, New York, 1994).
[85] V.Z. Fridman, A.A. Davydov, K. Titievsky, J. Catal. 222 (2004) 545-557.
[86] M. Sugantha, U.V. Varadaraju, G.V.S. Rao, J. Solid State Chem. 111 (1994) 33-40.
[87] C. Verissimo, F.M.S. Garrido, O.L. Alves, P. Calle, A. MartinezJuarez, J.E. Iglesias, J.M. Rojo, Solid State Ionics. 100 (1997) 127-134.
[88] J. Legget, Global Warming (Oxford University Press, New York, 1990).
[89] W.S. Broecker, Nature. 328 (1987) 123-126.
[90] H. Fujiwara, H. Hosokawa, K. Murakoshi, Y. Wada, S. Yanagida, T. Okada, H. Kobayashi, J. Phys. Chem. B. 101 (1997) 8270-8278.
[91] K.R. Thampi, J. Kiwi, M. Gratzel, Nature. 327 (1987) 506-508.
[92] T. Inoue, A. Fujishima, S. Konishi, K. Honda, Nature. 277 (1979) 637-638.
[93] B. Aurianblajeni, M. Halmann, J. Manassen, Solar Energy. 25 (1980) 165-170.
[94] K. Sayama, H. Arakawa, J. Photoch. Photobio. A. 94 (1996) 67-76.
[95] K. Sayama, H. Arakawa, J. Phys. Chem. 97 (1993) 531-533.
[96] K. Iizuka, Y. Kojima, A. Kudo, Shokubai. 51 (2009) 228-233.
[97] O. Ishitani, M.W. George, T. Ibusuki, F.P.A. Johnson, K. Koike, K. Nozaki, C.J. Pac, J.J. Turner, J.R. Westwell, Inorg. Chem. 33 (1994) 4712-4717.
[98] H. Hori, J. Ishihara, K. Koike, K. Takeuchi, T. Ibusuki, O. Ishitani, J. Photoch. Photobio. A. 120 (1999) 119-124.
[99] Y. Kohno, H. Hayashi, S. Takenaka, T. Tanaka, T. Funabiki, S. Yoshida, J. Photoch. Photobio. A. 126 (1999) 117-123.
[100] Y. Kohno, T. Yamamoto, T. Tanaka, T. Funabiki, J. Mol. Catal. A-Chem. 175 (2001) 173-178.
[101] Y. Kohno, T. Tanaka, T. Funabiki, S. Yoshida, Chem. Commun. (1997) 841-842.
[102] Y. Kohno, T. Tanaka, T. Funabiki, S. Yoshida, Chem. Lett. (1997) 993-994.
[103] Y. Kohno, T. Tanaka, T. Funabiki, S. Yoshida, J. Chem. Soc.-Faraday Trans. 94 (1998) 1875-1880.
[104] Y. Kohno, T. Tanaka, T. Funabiki, S. Yoshida, Phys. Chem. Chem. Phys. 2 (2000) 2635-2639.
[105] Y. Kohno, T. Tanaka, T. Funabiki, S. Yoshida, Phys. Chem. Chem. Phys. 2 (2000) 5302-5307.
[106] Y. Kohno, H. Ishikawa, T. Tanaka, T. Funabiki, S. Yoshida, Phys. Chem. Chem. Phys. 3 (2001) 1108-1113.
[107] K. Teramura, T. Tanaka, H. Ishikawa, Y. Kohno, T. Funabiki, J. Phys. Chem. B. 108 (2004) 346-354.
[108] K. Teramura, H. Tsuneoka, T. Shishido, T. Tanaka, Chem. Phys. Lett. 467 (2008) 191-194.
[109] Y. Fukuda, K. Tanabe, Bull. Chem. Soc. Jpn. 46 (1973) 1616-1619.
[110] H. Tsuji, T. Shishido, A. Okamura, Y.Z. Gao, H. Hattori, H. Kita, J. Chem. Soc.-Faraday Trans. 90 (1994) 803-807.
[111] Y. Yanagisawa, K. Takaoka, S. Yamabe, T. Ito, J. Phys. Chem. 99 (1995) 3704-3710.
[112] G. Busca, J. Lamotte, J.C. Lavalley, V. Lorenzelli, J. Am. Chem. Soc. 109 (1987)

5197-5202.
[113] O.Y. Feng, J.N. Kondo, K. Maruya, K. Domen, J. Chem. Soc.-Faraday Trans. 93 (1997) 169-174.
[114] G.W. Wang, H. Hattori, J. Chem. Soc.-Faraday Trans. I. 80 (1984) 1039-1047.

Table 1 Aerobic oxidation of various amines to corresponding imines using Nb_2O_5. [a]

Entry	Substrate	Product	T / h	Conv. (%)	Sel. (%) [b]
1			50	>99	97
1’	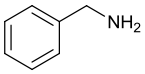	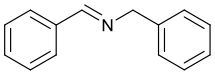	24	21	97
				0 [c]	– [c]
2	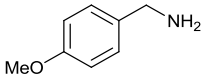	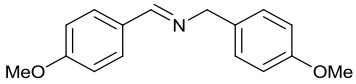	24	>99	99
2’			24	29	94
3	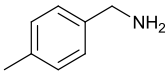	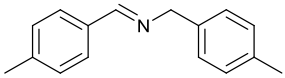	38	>99	95
3’			24	19	94
4	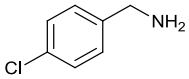	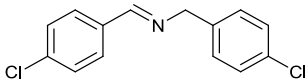	45	>99	98
4’			24	12	94
5	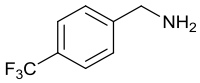	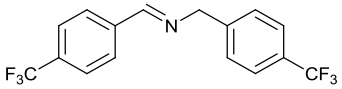	51	>99	96
6	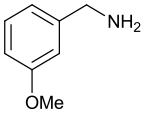	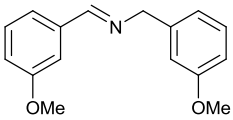	27	>99	95
6’			24	30	95
7	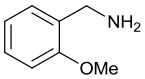	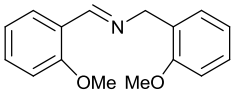	29	>99	94
7’			24	16	95
8	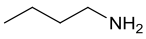	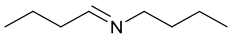	24	>99	61(14) [d]
9	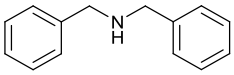	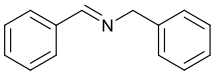	20	97	71 (23)
9’			24	16	70 (29)
10	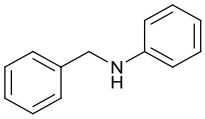	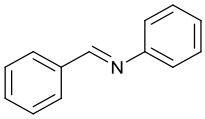	48	15	63 (21)
10’			24	2.5	86 (9)
11	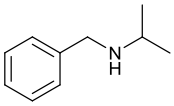	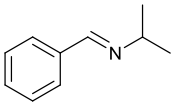	15	82	92 (5)
11’			24	47	91 (5)
12	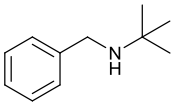	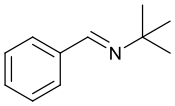	24	30	88 (7)
12’			24	13	89 (8)
13	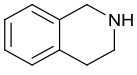	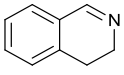	11	>99	92 (5) [e]
13’			24	47	85 (6) [e]
14	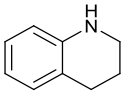	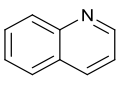	48	43	70 (4, 20) [f, g]
14’			24	4.2	84 (8) [g]

15	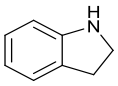	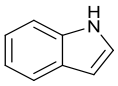	24	39	64 (13, 14) [h, i]
15’			24	2.4	87 (12) [h]

[a] Reaction condition: Nb_2O_5 (100 mg), substrate (5 mmol), benzene as a solvent (10 ml), λ > 300 nm (entries 1─15) or λ > 390 nm (entries 1’─15’), oxygen pressure (1 atm). [b] Selectivities to corresponding imines. Figures in parentheses show selectivities to benzaldehyde. [c] Without catalyst. Selectivities to [d] *N*,*N*-dibutylformamide, [e] isoquinoline, [f] 3,4-dihydroquinoline, [g] 3,4-dihydroquinoline-1(2*H*)-carbaldehyde, [h] indoline-1-carbaldehyde and [i] 10,11-dihydro-5*H*-dibenzo[*b*,*f*]azepine, respectively.

Figure captions

Figure 1. Time course of N_2 (circle) and N_2O (triangle) in the photo-SCR with NH_3 over TiO_2 JRC-TIO-11, Reaction condition; GHSV = 8000 h^{-1}, NO: 1000ppm, NH_3: 1000ppm, O_2: 2%, Ar balance

Figure 2. Action spectrum of photo-SCR (dot) and UV-Vis spectrum of JRC-TIO-11 (liner); reaction condition of action spectrum: NH_3: 1000ppm, NO: 1000ppm, O_2: 2%, flow rate: 100 ml/min.

Figure 3. FT-IR spectra of adsorbed species on TiO_2 in the photo-SCR with NH_3. (a) after introduction of NH_3, (b) after evacuation, (c) after introduction of NO in the dark, (d) under photo irradiation for 10 min, (e) for 30 min, (f) for 60 min, and (g) for 120 min.

Figure 4. ESR spectra of TiO_2 (a) after pretreatment, (b) after introduction of NH_3 in the dark, (c) under photo irradiation and (d) after introduction of NO in the dark.

Figure 5. Models of (a) $Ti_7O_{27}H_{26}$ fixed cluster and the optimized geometries, (b) NH_3-adsorbed $Ti_7O_{27}H_{26}$ fixed cluster, and (c) NH_3 dissociative adsorbed $Ti_7O_{27}H_{26}$ fixed cluster.

Figure 6. Energy levels around HOMO and LUMO for (a) $Ti_7O_{27}H_{26}$, (b) NH_3-adsorbed $Ti_7O_{27}H_{26}$, and (c) NH_3 dissociative adsorbed $Ti_7O_{27}H_{26}$.

Figure 7. Selected molecular orbitals of NH_3 dissociative adsorbed $Ti_7O_{27}H_{26}$ fixed cluster.

Figure 8. Action spectrum of photooxidation of 1-penanol (dot) and UV-Vis spectrum of Nb_2O_5 (liner). Reaction conditions of the action spectrum were as follows: 1-pentanol (10 ml), Nb_2O_5 (100 mg), 323 K, under 0.1 MPa of O_2, O_2 flow rate (2 cm^3 min^{-1}). Action spectrum of 1-pentanol photooxidation over Cu/Nb_2O_5, UV-Vis spectra of Cu/Nb_2O_5 and 1-pentanol adsorbed on Cu/Nb_2O_5, and difference spectrum between them.

Figure 9. FT-IR spectra of adsorbed species on Nb_2O_5 in the photo-reaction of adsorbed cyclohexanol with O_2. (a) cyclohexanol was exposed to Nb_2O_5 for 1 h and evacuated for 2 h, (b) under UV irradiation for 1, (c) 5 , (d) 7 , (e) 10 , (f) 15 and (g) 30 min. Nb_2O_5 was

evacuated at 773 K for 1 h and oxidized at 773 K with 10.7 kPa of O_2 and then evacuated at 773 K for 1 h before FT-IR measurements.

Figure 10. A) Model clusters of T-Nb_2O_5; $Nb_{12}O_{43}H_{26}$ (**1**) and alkoxide adsorbed on T-Nb_2O_5 (100); $Nb_{12}O_{42}H_{25}(OCH_3)$ (**2**). (B) Graphical illustrations of LUMO, HOMO and HOMO of **1** and **2**.

Figure 11. Energy diagram of the frontier orbitals of **1** and **2**.

Figure 12. Time dependence of the amount of CO evolution (●) and CH_4 consumption (▲) over MgO under photoirradiation.

Figure 13. Dependence of the amount of CO evolved by the photo-catalytic reaction (●) and by the heat treatment after photocatalytic reaction (▲) on the initial amount of introduced CO_2.

Figure 14. Difference IR spectra of the adsorbed species on MgO (a) after introduction of 3.9 kPa of CO_2 and evacuation, (b) after introduction of 5.1 kPa of H_2 and under photoirradiation for 18 h, and (c) after evacuation. The inset illustrates the difference spectrum between (a) and (b) in the region of 1800-1250 cm^{-1}, indicating the spectrum of adsorbate.

Figure 15. Difference IR spectra of the adsorbed species on MgO (a) after introduction of 3.9 kPa of CO_2 and evacuation, (b) after introduction of 5.2 kPa of CH_4 and under photoirradiation for 18 h, and (c) after evacuation. The inset illustrates the difference spectrum between (a) and (b) in the region of 1800-1250 cm^{-1}, indicating the spectrum of adsorbate.

Figure 16. Two bidentate species on MgO

Figure 17. Phosphorescence excitation spectra of MgO (a) after pretreatment, (b) after introduction of 33 μmol g-MgO^{-1} of CO_2 and (c) after introduction of 66 μmol g-MgO^{-1} of CO_2.

Scheme 1. Model of reaction, charge separation, and recombination over photocatalyst

Scheme 2. Reaction mechanism of photo-SCR with NH_3 over TiO_2

Scheme 3. Formation mechanism of NH_2 radical over TiO_2

Scheme 4. Reaction mechanism of alcohol photooxidation with molecular oxygen over Nb_2O_5

Scheme 5. Formation mechanism of alkyl carbon radical over Nb_2O_5

Scheme 6. Formation mechanism of amide radical radical over Nb_2O_5

Scheme 7. Reaction mechanism of CO_2 photo-reduction with H_2 or CH_4 over MgO

Scheme 8. Formation mechanism of CO_2^- or CO_3^- radical radical over MgO

Table 1. Aerobic oxidation of various amines to corresponding imines using Nb_2O_5.